IUST
Iran University of Science and Technology

Iranian Journal of Electrical and Electronic Engineering

Journal Homepage: ijeee.iust.ac.ir

2D Analytical Modeling of Magnetic Vector Potential in Surface Mounted and Surface Inset Permanent Magnet Machines

A. Jabbari*(C.A.)

Abstract: A 2D analytical method for magnetic vector potential calculation in inner rotor surface mounted and surface inset permanent magnet machines considering slotting effects, magnetization orientation and winding layout has been proposed in this paper. The analytical method is based on the resolution of Laplace and Poisson equations as well as Maxwell equation in quasi- Cartesian coordinate by using sub-domain method and hyperbolic functions. The developed method is applied on the performance computation of two prototypes surface mounted permanent magnet motors and two prototypes surface inset permanent magnet motors. A radial and a parallel magnetization orientation is considered for each type of motor. The results of these models are validated through FEM method.

Keywords: Analytical Modeling, Surface Mounted PM Machine, Surface Inset PM Machine, Sub-Domain Method, FEM.

1 Introduction

BRUSHLESS permanent magnet machines are interested in industrial applications due to their high efficiency, power density and robustness. An accurate prediction of airgap magnetic field distribution is necessary in order to calculate electromagnetic torque, back electromotive force and self or mutual inductance more precise. A variety of techniques including analytical and numerical methods has been conducted to evaluate the magnetic field distribution in electrical machines. Numerical methods like finite element method (FEM) give accurate results and are time-consuming especially in first step of design stage [1]-[2]. Analytical methods including conformal mapping [3]-[6], Magnetic Equivalent Circuit (MEC) [7]-[9], sub-domain model [10]-[26] and slot relative permeance calculation [27]-[28] are reported to model electrical machines and are useful in first step of performance evaluation and design optimization stage. The sub-domain model is more accurate than the other analytical models [7]. This method is developed based on solution of Laplace and Poisson equations in different regions by applying boundary conditions for electrical machines [10]-[26].

The focus of this paper is to develop an analytical model based on resolution of Laplace and Poisson equations in brushless surface mounted and surface inset permanent magnet machines by using the sub-domain method considering slotting effects, magnetization orientation and winding layout. It is shown that the developed model can effectively estimate magnetic field, electromagnetic torque, back electromotive force and self/mutual inductance. This model is applied on the performance calculation of four prototype brushless machines. It's shown that the results of analytical model are in close agreement with the results of FEM.

2 Problem Definition

The geometrical representation of the investigated brushless machines are shown in Fig. 1. The machines parameters including the rotor inner radius, R_1 rotor yoke radius, R_2, the rotor surface radius, R_3, the stator surface radius, R_4, the stator slot inner radius, R_5, the stator slot outer radius, R_6 and the stator yoke radius, R_7. Two different magnetization orientation including radial

Iranian Journal of Electrical & Electronic Engineering, 2017.
Paper first received 16 July 2017 and accepted 28 October 2017.
* The author is with the Department of Mechanical Engineering, Faculty of Engineering, Arak University, Arak, 38156-8-8849, Iran.
E-mail: a-jabbari@araku.ac.ir.
Corresponding Author: A. Jabbari.

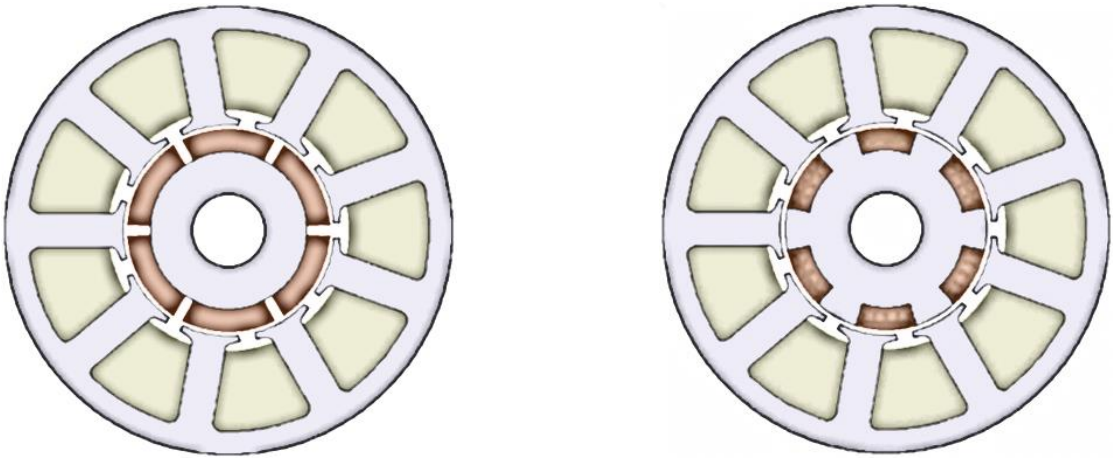

(a) (b)

Fig. 1 The schematic representation of (a) surface mounted, (b) surface inset permanent magnet machines.

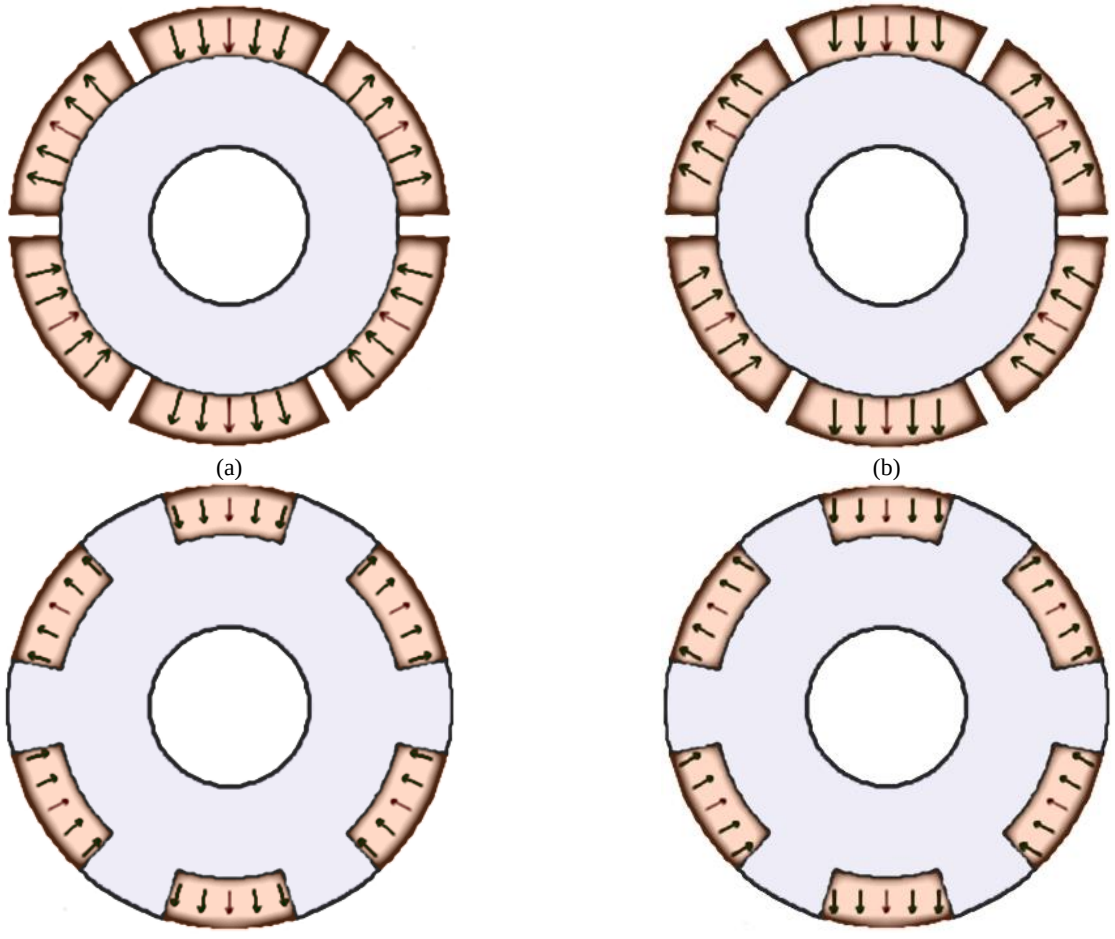

(a) (b)

(c) (d)

Fig. 2 Permanent magnet magnetization orientation, (a) surface-radial magnetization, (b) surface- parallel magnetization, (c) inset-radial magnetization, (d) inset- parallel magnetization.

and parallel magnetization for each topology are shown in Fig. 2.

The following assumptions are made in theoretical analysis:

- Permeability of rotor and stator cores are infinite;
- End effects are neglected;

The machine model is divided into four sub-domains. The stator which has two sub-domains including Q_1 slot regions (domain *j*) and Q_1 slot opening regions (domain *i*) and the airgap sub-domain (region *II*) are shown in Fig. 3. The rotor has one sub-domain including Q_2 permanent magnet regions (domain *I*) as shown in Fig. 4.

The angular position of the *i*-th stator slot, *i*-th stator

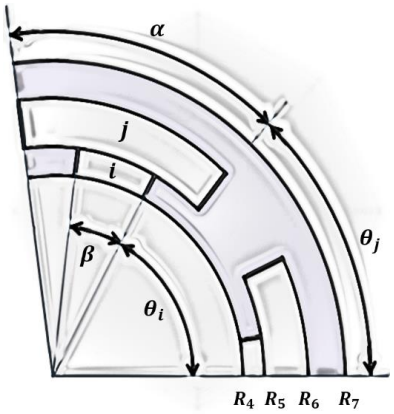

Fig. 3 The stator sub-domains including *j* and *i* regions.

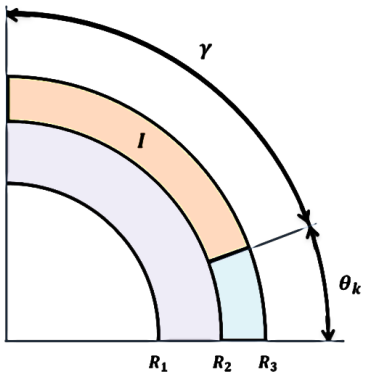

(a)

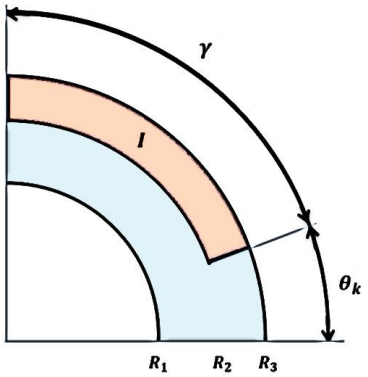

(b)

Fig. 4 The rotor sub-domains including *i* region.

slot opening, *i*-th permanent magnet are defined as (1), (2), and (3), respectively. A representation of α, β, and γ is shown in Fig. 3.

$$\theta_j = -\frac{\alpha}{2} + \frac{2i\pi}{Q_1} \quad \text{with} \quad 1 \le i \le Q_1 \tag{1}$$

$$\theta_i = -\frac{\beta}{2} + \frac{2i\pi}{Q_1} \quad \text{with} \quad 1 \le i \le Q_1 \tag{2}$$

$$\theta_I = -\frac{\gamma}{2} + \frac{2i\pi}{Q_2} \quad \text{with} \quad 1 \le i \le Q_2 \tag{3}$$

3 Magnetic Vector Potential Calculation

General solution of Laplace or Poisson equation in each sub-domain is developed in this section. The Laplace equation can be described in polar form as

$$\frac{\partial^2 A}{\partial r^2} + \frac{1}{r}\frac{\partial A}{\partial r} + \frac{1}{r^2}\frac{\partial^2 A}{\partial \theta^2} = 0 \quad \text{for} \quad \begin{cases} R_1 \le r \le R_2 \\ \theta_1 \le \theta \le \theta_2 \end{cases} \tag{4}$$

Replacing r by $R_1 e^{-t}$, one obtains

$$\frac{\partial^2 A}{\partial t^2} + \frac{\partial^2 A}{\partial \theta^2} = 0 \quad \text{for} \quad \begin{cases} ln\left(\frac{R_1}{R_2}\right) \le t \le 0 \\ \theta_1 \le \theta \le \theta_2 \end{cases} \tag{5}$$

The above equation has a quasi-Cartesian form instead of polar form. Therefore, it is possible to derive an analytical expression for magnetic vector potential based on hyperbolic functions.

3.1 Magnetic vector potential in the stator slot sub-domain (Region *j*)

The Poisson equation in the stator slot sub-domain is given by

$$\frac{\partial^2 A_j}{\partial t^2} + \frac{\partial^2 A_j}{\partial \theta^2} = -\mu_0 J \quad \text{for} \quad \begin{cases} t_1 \le t \le t_2 \\ \theta_j \le \theta \le \theta_j + \alpha \end{cases} \tag{6}$$

where $t_1 = ln\left(\frac{R_5}{R_6}\right)$, $t_2 = 0$ and J is slot current density.

Neumann boundary conditions at the bottom and at each side of the slot are obtained as

$$\left.\frac{\partial A_j}{\partial \theta}\right|_{\theta=\theta_j} = 0 \quad \text{and} \quad \left.\frac{\partial A_j}{\partial \theta}\right|_{\theta=\theta_j+\alpha} = 0 \tag{7}$$

$$\left.\frac{\partial A_j}{\partial t}\right|_{t=t_1} = 0 \tag{8}$$

The general solution of (6) using the separation of variables method is given by

$$\begin{aligned} A_j(t.\theta) = {} & a_0{}^j - \frac{1}{2}\mu_0 J_i\left(e^{-t_1}t + \frac{1}{2}e^{-2t+t_1}\right) \\ & + \sum_{h=1}^{\infty}\left(a_h{}^j \frac{\alpha}{h\pi}\frac{\cosh\left(\frac{h\pi}{\alpha}(t-t_1)\right)}{\sinh\left(\frac{h\pi}{\alpha}(t_2-t_1)\right)}\right) \\ & \times \cos\left(\frac{h\pi}{\alpha}(\theta-\theta_j)\right) \end{aligned} \tag{9}$$

where h is a positive integer and the coefficients $a_0{}^j$ and $a_h{}^j$ are determined based on the continuity and interface conditions.

The continuity of the magnetic vector potential between the sub-domain *j* and the region *i* leads to

$$\left.\frac{\partial A_j}{\partial t}\right|_{t=t_2} = f(\theta) = \begin{cases} \left.\frac{\partial A_i}{\partial t}\right|_{t=t_3} & for \quad \theta_i \le \theta \le \theta_i + \beta \\ 0 & \text{elsewhere} \end{cases} \tag{10}$$

Interface condition (10) gives

$$\mu_0 J_i \sinh(t_1) = \frac{1}{\alpha}\int_{\theta_j}^{\theta_j+\alpha} f(\theta).d\theta \tag{11}$$

$$a_h{}^j = \frac{2}{\alpha}\int_{\theta_j}^{\theta_j+\alpha} f(\theta).Cos\left(\frac{h\pi}{\alpha}(\theta-\theta_j)\right).d\theta \tag{12}$$

3.2 Magnetic vector potential in the stator slot opening sub-domain (Region *i*)

The Laplace equation in the stator second inner slot opening sub-domain is given by

$$\frac{\partial^2 A_i}{\partial t^2} + \frac{\partial^2 A_i}{\partial \theta^2} = 0 \quad \text{for} \quad \begin{cases} t_3 \le t \le t_4 \\ \theta_i \le \theta \le \theta_i + \beta \end{cases} \tag{13}$$

where $t_3 = ln\left(\frac{R_4}{R_5}\right)$ and $t_4 = 0$.

Neumann boundary conditions at the bottom and at each side of the slot are obtained as

$$\left.\frac{\partial A_i}{\partial \theta}\right|_{\theta=\theta_i} = 0 \quad \text{and} \quad \left.\frac{\partial A_i}{\partial \theta}\right|_{\theta=\theta_i+\beta} = 0 \tag{14}$$

The general solution of (13) using the separation of variables method is given by

$$A_i(t.\theta) = a_0^i + b_0^i t + \sum_{h=1}^{\infty}\left(\frac{\sinh\left(\frac{h\pi}{\beta}(t-t_4)\right)}{\sinh\left(\frac{h\pi}{\beta}(t_3-t_4)\right)}a_h^i + \frac{\sinh\left(\frac{h\pi}{\beta}(t-t_3)\right)}{\sinh\left(\frac{h\pi}{\beta}(t_4-t_3)\right)}b_h^i\right)\cos\left(\frac{h\pi}{\beta}(\theta-\theta_i)\right) \tag{15}$$

where *m* is a positive integer and the coefficients, a_0^i, b_0^i, a_h^i and b_h^i are determined based on the continuity and interface conditions.

The continuity of the magnetic vector potential between the sub-domain *l* and the regions *i* and *II* leads to

$$Ai(t_4.\theta) = AII(t_5.\theta) \quad \text{for} \quad \theta_i \le \theta \le \theta_i + \beta \tag{16}$$

$$Ai(t_3.\theta) = Aj(t_4.\theta) \quad \text{for} \quad \theta_i \le \theta \le \theta_i + \beta \tag{17}$$

Interface condition (16) gives

$$a_0{}^i = \frac{1}{\beta}\int_{\theta_i}^{\theta_i+\beta} AII(t_5.\theta).d\theta \tag{18}$$

$$b_m{}^i = \frac{2}{\beta}\int_{\theta_i}^{\theta_i+\beta} AII(t_5.\theta).\cos\left(\frac{h\pi}{\beta}(\theta-\theta_i)\right).d\theta \tag{19}$$

Interface condition (17) gives

$$a_0{}^i + \ln\left(\frac{R_5}{R_6}\right)b_0{}^i = \frac{1}{\beta}\int_{\theta_i}^{\theta_i+\alpha} Aj(t_4.\theta).d\theta \tag{20}$$

$$a_h{}^i = \frac{2}{\beta}\int_{\theta_i}^{\theta_i+\beta} Aj(t_4.\theta).\cos\left(\frac{h\pi}{\beta}(\theta-\theta_i)\right).d\theta \tag{21}$$

3.3 Magnetic vector potential in the air-gap sub-domain (Region *II*)

The Laplace equation in the internal airgap sub-domain is given by

$$\frac{\partial^2 A_{II}}{\partial t^2} + \frac{\partial^2 A_{II}}{\partial \theta^2} = 0 \quad \text{for} \quad \begin{cases} t_5 \le t \le t_6 \\ 0 \le \theta \le 2\pi \end{cases} \tag{22}$$

where $t_5 = ln\left(\frac{R_3}{R_4}\right)$ and $t_6 = 0$.

The general solution of (22) considering periodicity boundary conditions is obtained as

$$A_{II}(t.\theta) = \sum_{n=1}^{\infty}\left(\frac{1}{n}\frac{\cosh\left(n(t-t_6)\right)}{\sinh\left(n(t_5-t_6)\right)}a_n^{II} + \frac{1}{n}\frac{\cosh\left(n(t-t_5)\right)}{\sinh\left(n(t_6-t_5)\right)}b_n^{II}\right)\cos(n\theta) + \sum_{n=1}^{\infty}\left(\frac{1}{n}\frac{\cosh\left(n(t-t_6)\right)}{\sinh\left(n(t_5-t_6)\right)}c_n^{II} + \frac{1}{n}\frac{\cosh\left(n(t-t_5)\right)}{\sinh\left(n(t_6-t_5)\right)}d_n^{II}\right)\sin(n\theta) \tag{23}$$

where *n* is a positive integer.

The coefficients a_n^{II}, b_n^{II}, c_n^{II} and d_n^{II} are determined considering the continuity of magnetic vector potential between the internal airgap sub-domain *II* and the region *i* using a Fourier series expansion of interface condition (24) and (25) over the airgap interval.

The continuity of the magnetic vector potential between the internal airgap sub-domain *II* and the regionsi and *I* leads to

$$\left.\frac{\partial A_{II}}{\partial t}\right|_{t=t_5} = g(\theta) = \begin{cases} \left.\frac{\partial A_i}{\partial t}\right|_{t=t_4} & for \quad \theta_i \le \theta \le \theta_i + \beta \\ 0 & \text{elsewhere} \end{cases} \tag{24}$$

$$\left.\frac{\partial A_{II}}{\partial t}\right|_{t=t_6} = h(\theta) = \begin{cases} \left.\frac{\partial A_l}{\partial t}\right|_{t=t_7} & for \quad \theta_k \le \theta \le \theta_k + \gamma \\ 0 & \text{elsewhere} \end{cases} \tag{25}$$

Interface condition (24) gives

$$a_n^{II} = \frac{2}{2\pi}\int_{\theta_i}^{\theta_i+\beta} g(\theta).\cos(n\theta).d\theta \tag{26}$$

$$c_n^{II} = \frac{2}{2\pi}\int_{\theta_i}^{\theta_i+\beta} g(\theta).\sin(n\theta).d\theta \tag{27}$$

Interface condition (25) gives

$$b_n^{II} = \frac{2}{2\pi}\int_{\theta_k}^{\theta_k+\gamma} h(\theta).\cos(n\theta).d\theta \tag{28}$$

$$d_n^{II} = \frac{2}{2\pi}\int_{\theta_k}^{\theta_k+\gamma} h(\theta).\sin(n\theta).d\theta \tag{29}$$

3.4 Magnetic vector potential in the rotor permanent magnet sub-domain (Region *I*)

The Poisson equation in the rotor permanent magnet sub-domain is given by

$$\frac{\partial^2 A_I}{\partial t^2} + \frac{\partial^2 A_I}{\partial \theta^2} = -\frac{\mu_0}{r}\left(M_\theta - \frac{\partial M_r}{\partial \theta}\right) \quad \text{for} \quad \begin{cases} t_7 \le t \le t_8 \\ 0 \le \theta \le 2\pi \end{cases} \tag{30}$$

where $t_7 = ln\left(\frac{R_1}{R_2}\right)$ and $t_8 = 0$, M_θ and M_r are tangential and radial components of magnetization.

Radial Magnetization

The radial and tangential components of radial magnetization for surface mounted design in Fig. 2 (a) can express as

$$M_{rn} = \frac{4B_r}{\mu_0 n\pi}\sin\left(\frac{n\pi\alpha_p}{2}\right) \tag{31}$$

$$M_{\theta n} = 0 \tag{32}$$

where α_p is magnet pole width to magnet pitch ratio.
The radial and tangential components of radial magnetization for inset design in Fig. 2 (c) can express as

$$M_{rn} = \frac{4(-1)^k B_r}{\mu_0 n\pi}\sin\left(\frac{n\pi\alpha_p}{2\alpha_r}\right) \tag{33}$$

$$M_{\theta n} = 0 \tag{34}$$

Where α_r is rotor slot width to slot pitch.

Parallel Magnetization

The radial and tangential components of parallel magnetization for surface mounted design in Fig. 2 (b) can express as

$$M_{rn} = \frac{B_r}{\mu_0}\alpha_p\left[A_{1n}(\alpha_p) + A_{2n}(\alpha_p)\right] \tag{35}$$

$$M_{\theta n} = \frac{B_r}{\mu_0}\alpha_p\left[A_{1n}(\alpha_p) - A_{2n}(\alpha_p)\right] \tag{36}$$

where

$$A_{1n}(\alpha_p) = \frac{\sin\left((np+1)\frac{\pi\alpha_p}{2p}\right)}{(np+1)\frac{\pi\alpha_p}{2p}} \tag{37}$$

$$A_{2n}(\alpha_p) = \begin{cases} \dfrac{\sin\left((np-1)\frac{\pi\alpha_p}{2p}\right)}{(np-1)\frac{\pi\alpha_p}{2p}} & \text{for} \quad np \ne 1 \\ 1 & \text{for} \quad np = 1 \end{cases} \tag{38}$$

The radial and tangential components of parallel magnetization for inset design in Fig. 2 (d) can express as

$$M_{rn} = \frac{(-1)^k B_r}{\mu_0}\frac{\alpha_p}{\alpha_r}.\left[A_{1n}(\alpha_p.\alpha_r) - A_{2n}(\alpha_p.\alpha_r)\right] \tag{39}$$

$$M_{\theta n} = \frac{(-1)^k B_r}{\mu_0}\frac{\alpha_p}{\alpha_r}.\left[A_{1n}(\alpha_p.\alpha_r) - A_{2n}(\alpha_p.\alpha_r)\right] \tag{40}$$

where

$$A_{1n}(\alpha_p.\alpha_r) = \frac{\sin\left((np+\alpha_r)\frac{\pi\alpha_p}{2p\alpha_r}\right)}{(np+\alpha_r)\frac{\pi\alpha_p}{2p\alpha_r}} \tag{42}$$

$$A_{2n}(\alpha_p.\alpha_r) = \begin{cases} \dfrac{\sin\left((np-\alpha_r)\frac{\pi\alpha_p}{2p\alpha_r}\right)}{(np-\alpha_r)\frac{\pi\alpha_p}{2p\alpha_r}} & \text{for} \quad np \ne \alpha_r \\ 1 & \text{for} \quad np = \alpha_r \end{cases} \tag{43}$$

A. Surface Mounted Permanent Magnet Machine

For surface mounted design, Neumann boundary conditions at the bottom the permanent magnet are obtained as

$$\left.\frac{\partial A_I}{\partial t}\right|_{t=t_8} = 0 \tag{44}$$

The general solution of (31) using the separation of variables method is given by

$$A_I(t.\theta)=\sum_{n=1}^{\infty}\left(\begin{array}{l} a_n^I\dfrac{\cosh\left(n\left(t-t_8\right)\right)}{\cosh\left(n\left(t_7-t_8\right)\right)} \\ +X_n(t).\cos\left(\dfrac{n\pi\alpha_p}{2\alpha_r}\right)\end{array}\right).\cos(n\theta)$$

$$+\sum_{n=1}^{\infty}\left(\begin{array}{l} c_n^I\dfrac{\cosh\left(n\left(t-t_8\right)\right)}{\cosh\left(n\left(t_7-t_8\right)\right)} \\ +X_n(t).\sin\left(\dfrac{n\pi\alpha_p}{2\alpha_r}\right)\end{array}\right).\sin(n\theta) \quad (45)$$

$$X_n(t)=\left(1+\frac{1}{n}e^{(n+1)t}\right)f_n(t)$$

$$-\frac{\cosh\left(n\left(t-t_8\right)\right)}{\cosh\left(n\left(t_7-t_8\right)\right)}\left(1+\frac{1}{n}e^{(n+1)t_7}\right)f_n(t_7) \quad (46)$$

$$f_n(t)=\begin{cases}\mu_0\dfrac{npM_{rn}+M_{\theta n}}{1-np^2}R_1e^{-t} & \text{if } np\neq 1\\ -\mu_0\dfrac{M_{rn}+M_{\theta n}}{2}R_1e^{-t}ln\left(R_1e^{-t}\right) & \text{if } np=1\end{cases} \quad (47)$$

where n is a positive integer and the coefficients a_n^I and c_n^I are determined based on the continuity and interface conditions.

The continuity of the magnetic vector potential between the sub-domain *I* and the regions *II* leads to

$$A_I(t_7.\theta)=A_{II}(t_6.\theta) \quad (48)$$

Interface condition (36) gives

$$a_n^I=\frac{2}{2\pi}\int_0^{2\pi}A_{II}(t_6.\theta).\cos(n\theta).d\theta \quad (49)$$

$$c_n^I=\frac{2}{2\pi}\int_0^{2\pi}A_{II}(t_6.\theta).\sin(n\theta).d\theta \quad (50)$$

B. Surface Inset Permanent Magnet Machine

For surface inset design, Neumann boundary conditions at the bottom the permanent magnet are obtained as

$$\left.\frac{\partial A_I}{\partial t}\right|_{t=t_8}=0 \quad (51)$$

$$\left.\frac{\partial A_I}{\partial\theta}\right|_{\theta=\theta_k}=R_1e^{-t}(-1)^k B_r \quad \text{and}$$

$$\left.\frac{\partial A_I}{\partial\theta}\right|_{\theta=\theta_k+\gamma}=R_1e^{-t}(-1)^k B_r \quad (52)$$

The general solution of (31) using the separation of variables method is given by

$$A_I(t.\theta)=a_0^I-R_1e^{-t}(-1)^k B_r\left(\theta-\theta_k-\frac{\gamma}{2}\right)$$

$$+\sum_{h=1}^{\infty}\left(a_h^I\frac{\cosh\left(z\left(t-t_8\right)\right)}{\cosh\left(z\left(t_7-t_8\right)\right)}\right.$$

$$\left.+X_h^I(t).\cos(z\varphi_i)\right)\times\cos\left(z\left(\theta-\theta_k\right)\right) \quad (53)$$

$$X_h^I(t)=\begin{cases}\mu_0\dfrac{h\pi M_{rh}+M_{\theta h}}{\gamma z^2\left(1-z^2\right)}R_1\left(e^{-t}+\dfrac{1}{z}e^{zt}\right) & \text{if } h=1,3,5,\ldots\\ 0 & \text{if } h=2,4,6,\ldots\end{cases} \quad (54)$$

where $z=h\pi/\gamma$, h is a positive integer and the coefficients $a_0{}^I$ and $a_h{}^I$ are determined based on the continuity and interface conditions.

The continuity of the magnetic vector potential between the sub-domain *I* and the regions *II* leads to

$$A_I(t_7.\theta)=A_{II}(t_6.\theta) \quad (55)$$

Interface condition (36) gives

$$a_0^I=R_2(-1)^k B_r\left(\theta-\theta_k-\frac{\gamma}{2}\right)+\frac{1}{\gamma}\int_{\theta_k}^{\theta_k+\gamma}A_{II}(t_6.\theta).d\theta \quad (56)$$

$$a_n^I=\frac{2}{\gamma}\int_{\theta_k}^{\theta_k+\gamma}A_{II}(t_6.\theta).\cos\left(z\left(\theta-\theta_k\right)\right).d\theta \quad (57)$$

4 Performance Calculation and Model Evaluation

4.1 Performance Computation

The electromagnetic torque is obtained using the Maxwell stress tensor and expressed as

$$T_e=\frac{L_s}{\mu_0}\int_0^{2\pi}BI_r(t_e.\theta).BI_\theta(t_e.\theta).d\theta \quad (58)$$

where L_s is the axial length of the motor and t_e is calculated by

$$t_e=ln\left(\frac{R_2}{R_e}\right) \quad \text{and} \quad R_e=\frac{\left(R_2+R_3\right)}{2} \quad (59)$$

For single layer winding, the phase flux vector is calculated by

$$\begin{bmatrix}\psi_a\\ \psi_b\\ \psi_c\end{bmatrix}=N_cC^T\begin{bmatrix}\varphi_1 & \varphi_2 & \varphi_3 & \ldots & \varphi_{Q_2}\end{bmatrix} \quad (60)$$

where N_c, is the number of conductors in the stator slot, C is a matrix connection between the stator slots and phase connections, and φ is the slot flux.

For the stator slots, φ is given by

$$\varphi_i=-\frac{L_sR_4{}^2}{k_fS}\int_0^{\beta}\int_0^{t_8}A_{mi}(t.\theta).e^{-2t}.dt.d\theta \quad (61)$$

where k_f, is the stator fill factor and S is the area of the stator slot.
For double layer winding, the phase flux vector is calculated by

$$\begin{bmatrix}\psi_a\\ \psi_b\\ \psi_c\end{bmatrix}=\begin{bmatrix}\psi 1_a\\ \psi 1_b\\ \psi 1_c\end{bmatrix}+\begin{bmatrix}\psi 2_a\\ \psi 2_b\\ \psi 2_c\end{bmatrix} \tag{62}$$

where

$$\begin{bmatrix}\psi 1_a\\ \psi 1_b\\ \psi 1_c\end{bmatrix}=\frac{N_c}{2}C_1^T\begin{bmatrix}\varphi_{11} & \varphi_{12} & \varphi_{13} & \cdots & \varphi_{1Q_2}\end{bmatrix} \tag{63}$$

and

$$\begin{bmatrix}\psi 2_a\\ \psi 2_b\\ \psi 2_c\end{bmatrix}=\frac{N_c}{2}C_2^T\begin{bmatrix}\varphi_{21} & \varphi_{22} & \varphi_{23} & \cdots & \varphi_{2Q_2}\end{bmatrix} \tag{64}$$

For the stator slots, φ is given by

$$\varphi_{1i}=-\frac{2L_s{R_4}^2}{k_f S}\int_0^{\frac{\beta}{2}}\int_0^{t_8}A_{mi}(t.\theta).e^{-2t}.dt.d\theta \tag{65}$$

$$\varphi_{2i}=-\frac{2L_s{R_4}^2}{k_f S}\int_{\frac{\beta}{2}}^{\beta}\int_0^{t_8}A_{mi}(t.\theta).e^{-2t}.dt.d\theta \tag{66}$$

The back-EMF of phase A is given by

$$E_a=\omega\frac{d\psi_a}{d\theta_r} \tag{67}$$

where ω is the rotor angular speed and ψ_a is flux linkage per phase A.
The stator inductance (self-inductance) of phase A is given by

$$L=\frac{\psi_a}{I_A} \tag{68}$$

where I_A is the peak current in phase A.
The mutual inductance of phase A and phase B, is given by

$$M=\frac{N\varphi_{AB}}{I_B} \tag{69}$$

where N, is the number of phase turns, φ_{AB} is magnetic flux in phase A and I_B is the peak current in phase B.

4.2 Model Evaluation

In this section, the presented analytical model is used to study the magnetic flux density, electromagnetic torque, back- electromotive force, self-inductance and mutual inductance of four prototype motors. The results of analytical method are then verified by the results of finite element method. A 2D model of the studied brushless permanent magnet motor is shown in Fig. 1 and the motor parameters are given in Table 1. The matrix connection between the stator slots and phase connections of each layer for the investigated motors are given by

$$C_1=\begin{bmatrix}0&-1&0&0&-1&0&0&-1&0&0&-1&0\\ -1&0&0&-1&0&0&-1&0&0&-1&0&0\\ 0&0&-1&0&0&-1&0&0&-1&0&0&-1\end{bmatrix}$$

$$C_2=\begin{bmatrix}1&0&0&1&0&0&1&0&0&1&0&0\\ 0&0&1&0&0&1&0&0&1&0&0&1\\ 0&1&0&0&1&0&0&1&0&0&1&0\end{bmatrix}$$

Table 1 Parameters of the investigated motors.

Symbol	Quantity	Surface mounted machine	Surface inset machine
R_1	Inner radius of the rotor slot	5mm	5mm
R_2	Outer radius of the rotor slot	11.3mm	11.3mm
R_3	Inner radius of the stator	14.5mm	14.5mm
R_4	Outer radius of the stator inner slot opening	15mm	15mm
R_5	Outer radius of the stator inner slot	16mm	16mm
R_6	Inner radius of the stator outer slot	28.5mm	28.5mm
R_7	Outer radius of the stator outer slot	32mm	32mm
θ_i	Angular position of the first rotor slot	35	35
θ_j	Angular position of the first stator slot opening	26	26
θ_k	Angular position of the second stator slot opening	12	12
α	The first stator slot opening angle	30	30
β	The second stator slot opening angle	8	8
γ	The rotor slot angle	54	36
p	Pole pairs-number	6	6
Q_1	Number of stator slots	9	9
B_r	Remanence of the permanent magnets	1.2T	1.2T
L_s	Axial length	35mm	35mm

2D finite element method is applied on performance calculation of the investigated motors. Magnetic field distribution in the motor is represented in Fig. 5. An Open circuit comparison of analytical and numerical results of radial flux density and cogging torque of the investigated motors are shown in Fig. 6 and Fig. 7, respectively. An on load analytical and numerical comparison of, radial flux density, electromagnetic torque, back-electromagnetic force, self-inductance and mutual inductance in the investigated motor are shown in Fig. 8, Fig. 9, Fig. 10, Fig. 11 and Fig. 12, respectively. The investigated on load condition are given in Table 2.

The open circuit and on load radial components of the flux density distribution in the middle of the air gap (at r=12.9 mm) are shown in Fig. 6 and Fig. 8, respectively. The effect of the surface mounted and surface inset topology on the radial component waveform of the flux density is clear. The effect of slot opening on the flux density waveform in these two topologies is very clear. However, in case of surface inset machine, the flux density waveforms distortions at the locations of the rotor slots diminished. The analytical results are in an excellent agreement with the results of finite element method. It can be seen that the presented 2D analytical model can compute the cogging torque with an excellent precision for surface mounted and surface inset machine.

Fig. 9 shows the electromagnetic torque waveforms in terms of rotor position for different magnetization orientation in the surface mounted and surface inset topologies. At each rotor position, the current values in the different slots updated to have a sinusoidal current waveform. It is obvious that the radial surface mounted machine and the parallel surface mounted machine produce an average torque of about 1.156 Nm and 1.137 Nm, respectively. In case of surface inset machines, an average electromagnetic torque of about 0.564 Nm and 0.617 Nm can be seen for radial and parallel design, respectively. The average torque decreases slightly at the locations of the stator slot-openings. We can also see the effect of magnetization orientation on the torque ripple. In case of these two topology, the effect of cogging torque, slot opening and magnetization orientation and PM arrangement on torque ripples is evident. Once again, it can be seen that the analytical results are in close agreement with the numerical

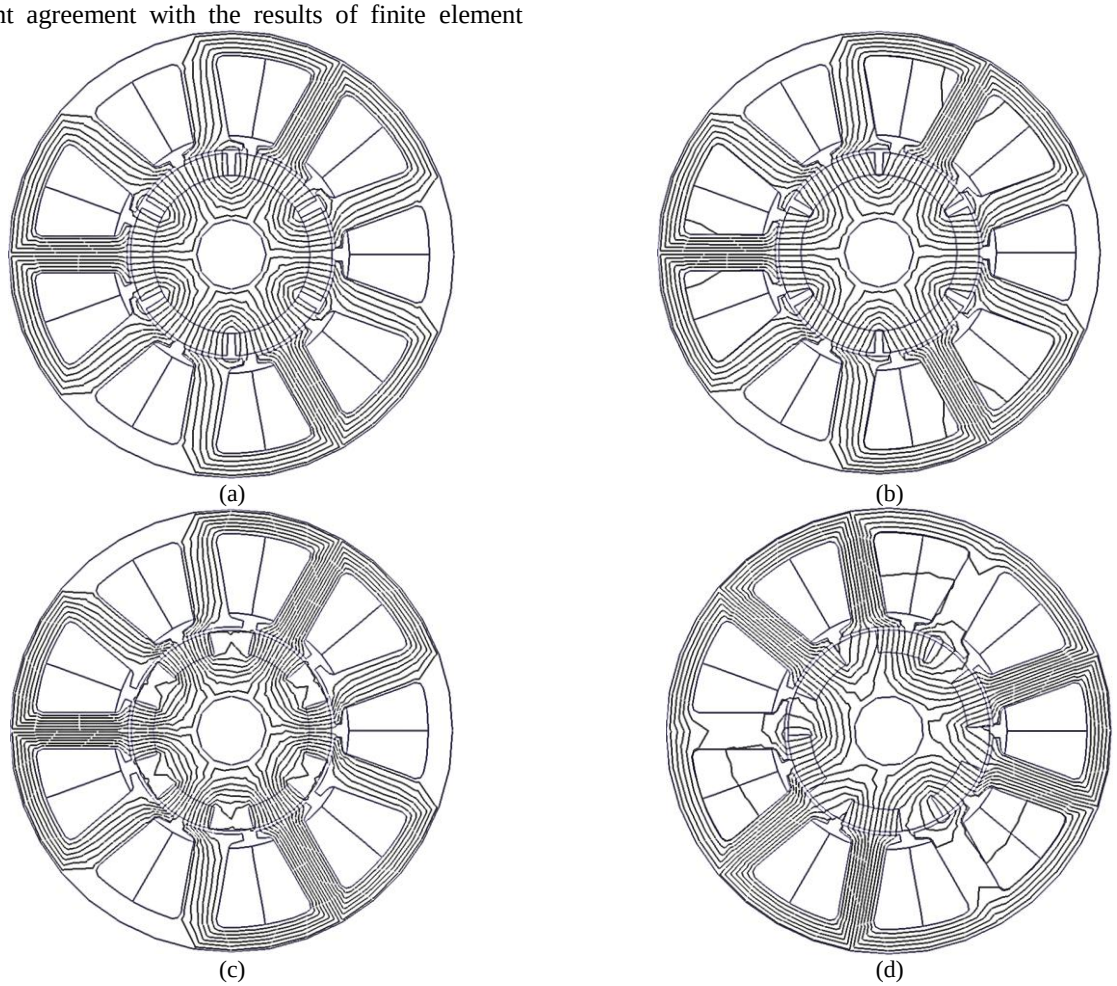

Fig. 5 Magnetic flux distribution in the investigated motors a) radial magnetized surface mounted motor, b) parallel magnetized surface mounted motor, c) radial magnetized surface inset motor and d) parallel magnetized surface inset motor.

rotor angular position for a rotating speed 1000 rpm are compered in Fig. 10. In case of surface mounted machines, the harmonic distortion of the back-EMF waveforms are less than that of surface inset machines.

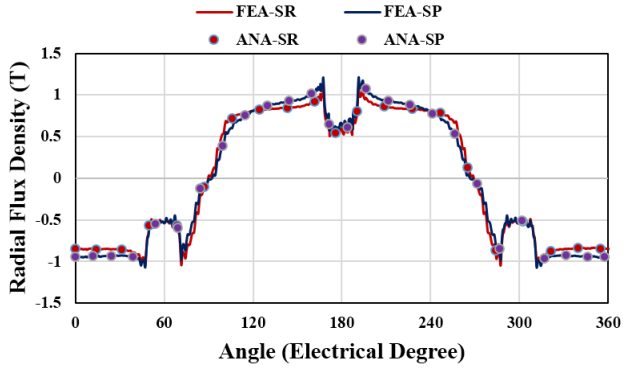

(a)

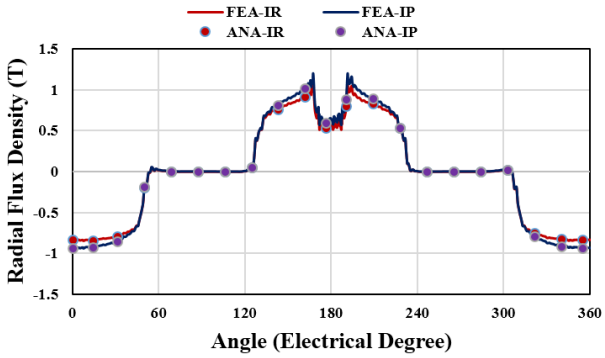

(b)

Fig. 6 Open circuit analytical and numerical comparison of radial flux density for the investigated motors a) surface mounted motors and b) surface inset motors.

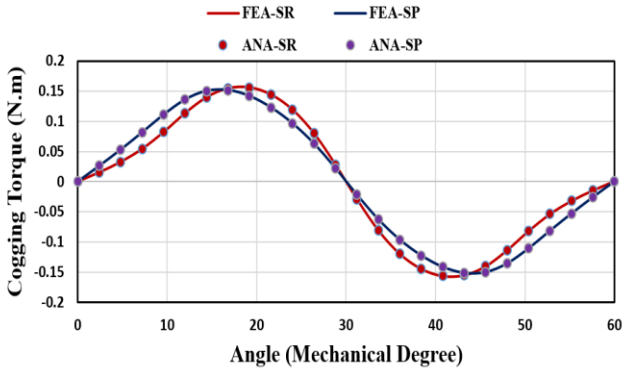

(a)

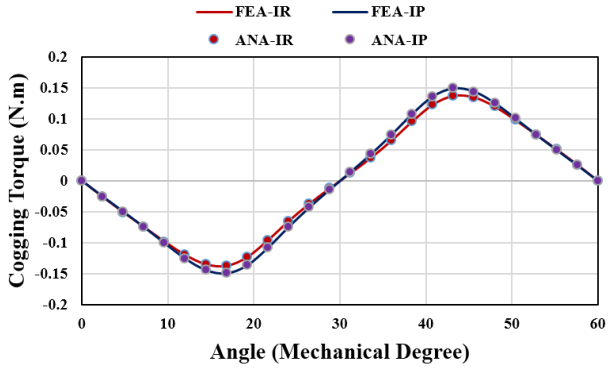

(b)

Fig. 7 Open circuit analytical and numerical comparison of cogging torque for the investigated motors a) surface mounted motors and b) surface inset motors.

Table 2 the investigated on load conditions.

Rated Power (W)	Rated Speed (RPM)	Line to Line Voltage (V)	Frequency (Hz)	Ambient temperature (°C)	Temperature rise (°C)
150	1000	120	50	22	60

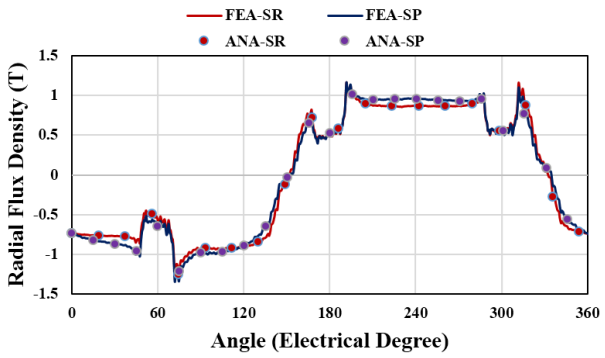

(a)

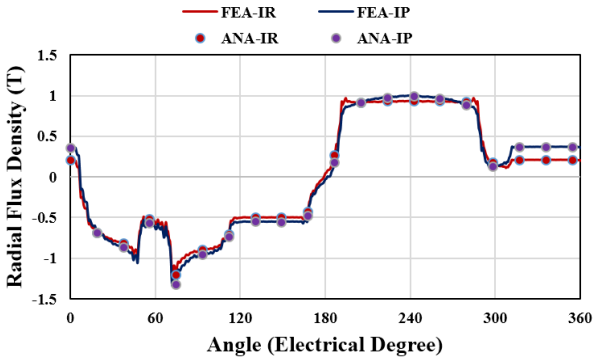

(b)

Fig. 8 On load analytical and numerical comparison of radial flux density for the investigated motors a) surface mounted motors and b) surface inset motors.

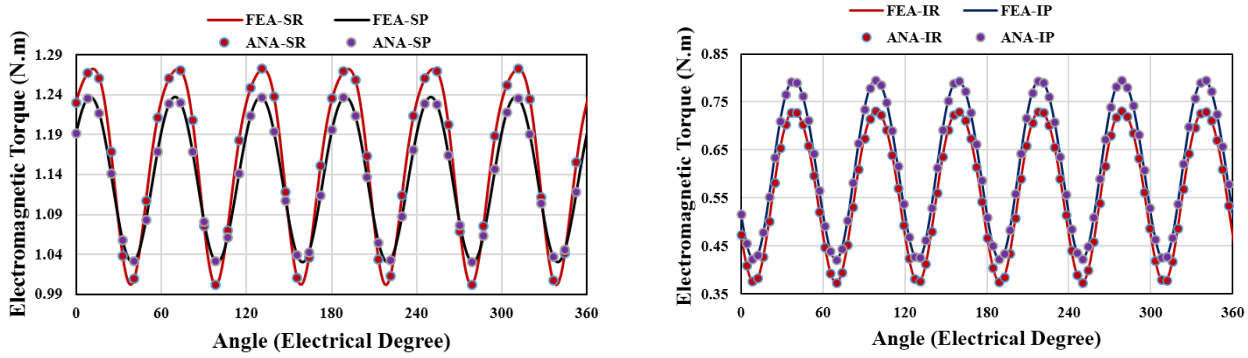

(a) (b)

Fig. 9 On load analytical and numerical comparison of electromagnetic torque for the investigated motors a) surface mounted motors and b) surface inset motors.

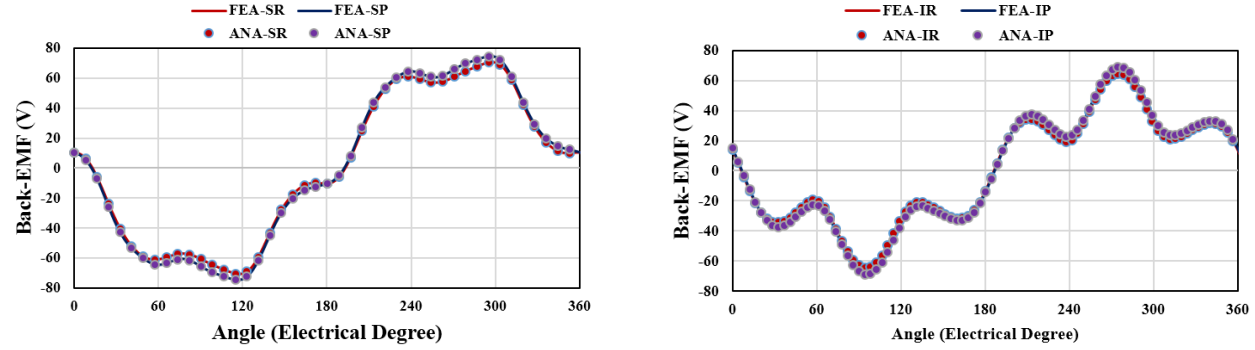

(a) (b)

Fig. 10 On load analytical and numerical comparison of Back-EMF for the investigated motors a) surface mounted motors and b) surface inset motors.

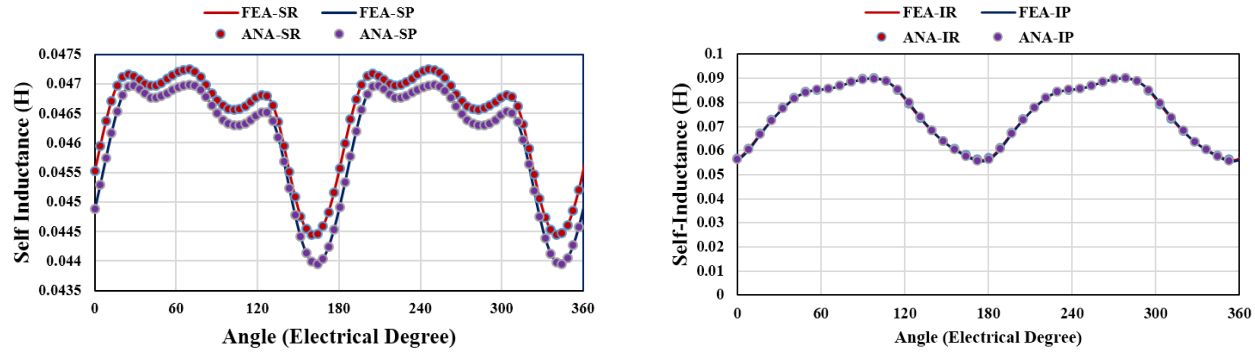

(a) (b)

Fig. 11 On load analytical and numerical comparison of self-inductance for the investigated motors a) surface mounted motors and b) surface inset motors.

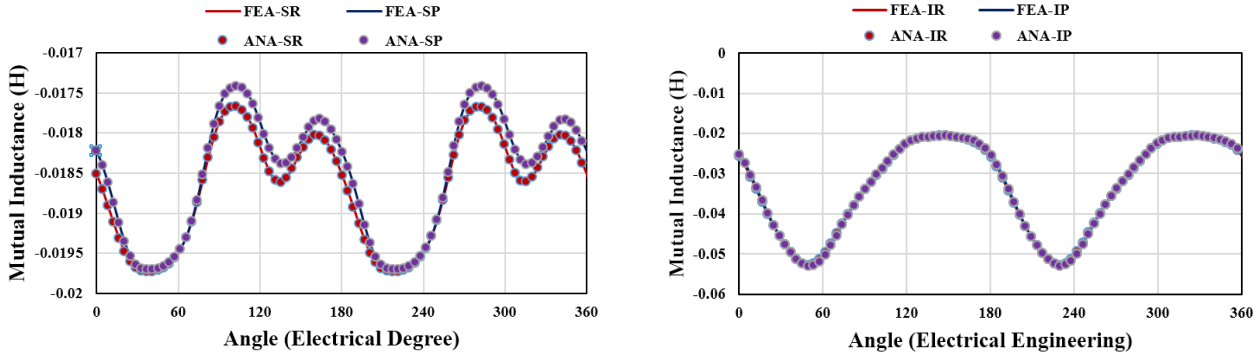

(a) (b)

Fig. 12 On load analytical and numerical comparison of mutual inductance for the investigated motors a) surface mounted motors and b) surface inset motors.

5 Conclusion

A general analytical model for performance prediction in brushless surface mounted and surface inset permanent magnet machines considering slotting effects, magnetization orientation and winding layout has been developed in this paper. Fourier analysis method based on sub-domain method and hyperbolic functions is applied to derive analytical expressions for calculation of magnetic vector potential, magnetic flux density, electromagnetic torque, back-electromotive force and self/mutual inductance in these machines. This model is applied for performance computation of four prototype motors and the results of proposed model are verified thanks to FEM results.

Acknowledgment

This research is carried out based on a research project which has been financially supported by the office of vice chancellor for research of Arak University with contact number of 93/8469.

References

[1] A. Jabbari, M. Shakeri, S. A. Nabavi Niaki, "Pole shape optimization of permanent magnet synchronous motors using the reduced basis technique," *Iranian Journal of Electrical and Electronic Engineering*, Vol. 6, No. 1, pp. 48-55, 2010.

[2] A. Jabbari, M. Shakeri, A. S. Gholamian, "Rotor pole shape optimization of permanent magnet brushless DC motors using the reduced basis technique," *Advances in Electrical and Computer Engineering*, Vol. 9, No. 2, pp. 75–81, 2009.

[3] Z. Q. Zhu and D. Howe, "Instantaneous magnetic-field distribution in brushless permanent-magnet dc motor, part III: Effect of slotting," *IEEE Trans. Magn*., Vol. 29, No. 1, pp. 143–151, Jan. 1993.

[4] M. Markovic, M. Jufer, and Y. Perriard, "Reducing the cogging torque in brushless dc motors by using conformal mappings," *IEEE Trans. Magn*., Vol. 40, No. 2, pp. 451–455, Mar. 2004.

[5] D. Zarko, D. Ban, and T. A. Lipo, "Analytical calculation of magnetic field distribution in the slotted air gap of a surface permanent-magnet motor using complex relative air-gap permeance," *IEEE Trans. Magn*., Vol. 42, No. 7, pp. 1828–1837, Jul. 2006.

[6] K. Boughrara, D. Zarko, R. Ibtiouen, O. Touhami, and A. Rezzoug, "Magnetic field analysis of inset and surface-mounted permanent- magnet synchronous motor using Schwarz-Christoffel transformation," *IEEE Trans. Magn*., Vol. 45, No. 8, pp. 3166–3168, Aug.2009.

[7] E. Ilhan, B. L. J. Gysen, J. J. H. Paulides and E. A. Lomonova "Analytical Hybrid Model for Flux Switching Permanent Magnet Machines," *IEEE Trans. Magnetics*., Vol. 46, No. 6, pp. 1762-1765, June 2010.

[8] Y. Tang, T.E.Motoasca, J.J.H. Paulides, and E.A. Lomonova"Analytical modeling of flux-switching machines using variable global reluctance networks". In Electrical Machines (ICEM), *2012 XXth International Conference on*, pp. 2792-2798, Sep. 2012.

[9] W. Hua, G. Zhang, M. Cheng and J. Dong "Electromagnetic Performance Analysis of Hybrid-Excited Flux-Switching Machines by a Nonlinear Magnetic Network Model," *IEEE Trans. Magnetics*., Vol. 47,No. 10, pp. 3216-3219, October 2011.

[10] Q. Gu and H. Gao, "Effect of slotting in PM electrical machines," *Elect. Mach. Power Syst*., Vol. 10, pp. 273–284, 1985.

[11] N. Boules, "Prediction of no-load flux density distribution in permanent magnet machines," *IEEE Trans. Ind. Appl*., Vol. IA-21, No. 3, pp. 633–643, Jul./Aug. 1985.

[12] B. Ackermann and R. Sottek, "Analytical modeling of the cogging torque in permanent magnet motors," Elect. Eng., Vol. 78, No. 2, pp. 117–125, Mar. 1994.

[13] A. Radun, "Analytical calculation of the switched reluctance motor's unaligned inductance," *IEEE Trans. Magn*., Vol. 35, No. 6, pp. 4473–4481, Nov. 1999.

[14] K. F. Rasmussen, H. D. John, T. J. E. Miller, M. I. McGilp, and O. Mircea, "Analytical and numerical computation of air-gap magnetic field in brushless motors with surface permanent magnet," *IEEE Trans. Magn*., Vol. 36, No. 6, pp. 1547–1554, Nov./Dec. 2000.

[15] X. Wang, Q. Li, S. Wang, and Q. Li, "Analytical calculation of air-gap magnetic field distribution and instantaneous characteristics of brushless dc motors," *IEEE Trans. Energy. Convers*., Vol. 18, No. 3, pp. 386–391, Sep. 2003.

[16] Z. J. Liu and J. T. Li, "Analytical solution of air-gap field in permanent magnet motors taking into account the effect of pole transition over slots," *IEEE Trans. Magn*., Vol. 43, No. 10, pp. 3872–3882, Oct. 2007.

[17] Z. J. Liu, J. T. Li, and Q. Jiang, "An improved analytical solution for predicting magnetic forces in permanent magnet motors," *J. Appl. Phys*., Vol. 103, No. 7, 2008.

[18] Z. J. Liu and J. T. Li, "Accurate prediction of magnetic field and magnetic forces in permanent magnet motor using an analytical solution," *IEEE Trans. Energy. Convers*., Vol. 23, No. 3, pp. 717–726, Sep. 2008.

[19] P. Kumar and P. Bauer, "Improved analytical model of a permanent magnet brushless dc motor," *IEEE Trans. Magn*., Vol. 44, No. 10, pp. 2299–2309, Oct. 2008.
[20] T. Lubin, S. Mezani, and A. Rezzoug"Exact analytical method for magnetic field computation in the air gap of cylindrical electrical machines considering slotting effects," *IEEE Trans. on Magnetics*, Vol. 46, No. 4, pp.1092-1099, 2010
[21] B. L. J. Gysen, E. Ilhan, K. J. Meessen, J. J. H. Paulides and E. A. Lomonova, "Modeling of Flux Switching Permanent Magnet Machines With Fourier Analysis," *IEEE Trans. Magnetics*., Vol. 46, No. 6, pp. 1499-1502, June 2010.
[22] K. Boughrara, R. Ibtiouen, and T. Lubin, "Analytical prediction of magnetic field in parallel double excitation and spoke-type permanent-magnet machines accounting for tooth-tips and shape of polar pieces," *IEEE Trans. on Magnetics*, Vol. 48, No. 7, pp.2121-2137, 2012.
[23] K. Boughrara, T. Lubin, and R. Ibtiouen, "General subdomain model for predicting magnetic field in internal and external rotor multiphase flux-switching machines topologies," *IEEE Trans. on Magnetics*, Vol. 49, No. 10, pp.5310-5325, 2013.
[24] T.L. Tiang, D. Ishak, and M.K.M. Jamil, "Complete subdomain model for surface-mounted permanent magnet machines," *In Energy Conversion (CENCON), 2014 IEEE Conference on*, pp. 140-145, October 2014.
[25] X. Liu, H. Hu, J. Zhao, A. Belahcen, L. Tang and L. Yang, "Analytical Solution of the Magnetic Field and EMF Calculation in Ironless BLDC Motor." *IEEE Trans. on Magnetics*, Vol. 52, No. 2, pp.1-10, 2016.
[26] B. Dianati, H. Heydariand S.A. Afsari, "Analytical Computation of Air-Gap Magnetic Field in a Viable Superconductive Magnetic Gear," *IEEE Trans. on Applied Superconductivity*, Vol. 26, No. 6, pp.1-12, 2016.
[27] B. Gaussens, E. Hoang, O. de la Barriere, J. Saint-Michel and M. Gabsi, "Analytical Approach for Air-gap Modeling of Field-Excited Flux- Switching machine: No-load Operation," *IEEE Trans. Magnetics*., Vol. 48, No. 9, pp. 2505-2517, 2012.
[28] B. Gaussens, E. Hoang, O. de la Barriere, J. Saint-Michel, P. Manfe, M. Lecrivain and M. Gabsi, "Analytical Armature Reaction Field Prediction in Field-Excited Flux-Switching Machines using an Exact Relative Permeance Function," *IEEE Trans. Magnetics*., Vol. 49, No. 1, pp.628-641, 2013.

A. Jabbari is an assistant professor in Mechanical Engineering Department at Arak University, Arak, Iran. He obtained a BSc degree in Mechanical Engineering from Iran University of Science and Technology in 2002. He received his MSc and PhD degrees both in Mechanical engineering from Mazandran University in 2004 and 2009, respectively. His research interests include renewable energy, electric machines, mechatronic systems and metal forming.